JOURNAL OF GUIDANCE, CONTROL, AND DYNAMICS
Vol. 23, No. 1, January–February 2000

Dual Payload Ascent Trajectory Optimization with a Splash-Down Constraint

Nicolas Weigel* and Klaus H. Well†
University of Stuttgart, 70550 Stuttgart, Germany

Optimal ascent trajectories for a multistage launch vehicle for dual payload problems are investigated. The optimization problems are formulated as multiphase problems with boundary and path constraints. Solutions are obtained using a direct multiple shooting method. Emphasis is placed on enforcing the splash-down constraint for the burned-out lower stage by simulating its return trajectory. The sensitivity of the optimization results with respect to the splash-down location is analyzed.

Introduction

DUAL payload capability of launch vehicles reduces the cost per satellite and utilizes the launch vehicle to its fullest extent. The purpose of this paper, therefore, is to investigate the performance capability of a particular launch system for two payload/target-orbit combinations using trajectory optimization as the mathematical tool. This approach is particularly well suited to determine optimal injection strategies in view of multiple target orbits and conflicting path constraints, such as heat-flux constraints at payload fairing jettisoning and splash-down constraints for the burned-out lower stage of the vehicle, the latter constraint being enforced to reduce space debris. Resolving the conflicts and still providing optimality make this problem difficult to solve. The trajectory optimization problem can be cast as a multiphase problem with boundary constraints enforced at the end of each phase and path constraints enforced pointwise during each phase. Although the results presented are for a specific vehicle, the general approach can be used for any vehicle having multiple stages or multiple intermediate boundary and/or path constraints.

There have been several papers that have reported about the performance of particular vehicles that used trajectory optimization, for example, Refs. 1–5. In addition, the trajectory design of aerospace vehicles, in general, and of advanced launch vehicles, in particular, has sparked the development of general optimization codes[6–10] that can be used for the performance analysis. None of the papers mentioned so far, however, has addressed the issue of multiple payloads although multiple payloads are launched in practice. In addition, in Refs. 2, 4, and 5, the splash-down constraint for the burned-out lower stage of the vehicle under consideration has been formulated as an intermediate boundary constraint on perigee altitude of the osculating orbit after burnout of the lower stage. It will be shown that a complete simulation of the return trajectory is needed for accurate predictions of the splash-down position.

Problem Statement

This paper investigates optimal ascent trajectories for an Ariane 5-type launch vehicle for dual payload problems. Two cases are studied. In the first case, a first payload weighing 3000 kg is to be injected into a low Earth orbit (LEO) with an altitude of 600 km and an inclination of 7 deg. A second payload is then to be maximized into a geostationary transfer orbit (GTO) with the same inclination. The second problem consists of transporting a 4000-kg payload into a sun-syncronous orbit (SSO) with an altitude of 800 km and a second payload weighing 4000 kg into a circular orbit with an altitude of 800 km and minimal inclination. The most important mission data are summarized in Table 1.

Mathematical Model

Equations of Motion

The kinematic and dynamic equations describing the translational motion of a vehicle over a rotating planet are

$$\frac{\mathrm{d}}{\mathrm{d}t}\boldsymbol{R} = \frac{\mathrm{d}}{\mathrm{d}t}\begin{bmatrix} R \\ \lambda \\ \delta \end{bmatrix}_L = m\begin{bmatrix} V_R \\ (V_\lambda / R\cos\delta) - \Omega_E \\ V_\delta / R \end{bmatrix} \tag{1}$$

$$\frac{\mathrm{d}}{\mathrm{d}t}\boldsymbol{V} = \frac{\mathrm{d}}{\mathrm{d}t}\begin{bmatrix} V_R \\ V_\lambda \\ V_\delta \end{bmatrix}_L = \frac{1}{R}\begin{bmatrix} V_\lambda^2 + V_\delta^2 \\ V_\lambda(V_\delta \tan\delta - V_R) \\ -V_\lambda^2\tan\delta - V_R V_\delta \end{bmatrix} + \boldsymbol{g} + \frac{1}{m}\boldsymbol{F}_{\mathrm{aero}} + \frac{1}{m}\boldsymbol{F}_{\mathrm{prop}} \tag{2}$$

The equations are evaluated in the local axis system given in Fig. 1. $\boldsymbol{R}$ is the vehicle's position vector. $\boldsymbol{V}$ is the inertial velocity, with components V_R, V_λ, and V_δ aligned with the axes x_L, y_L, and z_L, respectively. Ω_E is the rotation of the Earth. The external loads $\boldsymbol{g}$, $\boldsymbol{F}_{\mathrm{aero}}$ and $\boldsymbol{F}_{\mathrm{prop}}$ are described subsequently.

Aerodynamic Forces

The aerodynamic forces are described most conveniently in the body-fixed system B shown in Fig. 2 using the components A (axial force), Y (side force), and N (normal force). These are obtained by multiplying dynamic pressure q, reference area $S = 22.0\ \mathrm{m}^2$, and the coefficients c_A, c_Y, and c_N respectively,

$$\boldsymbol{F}_{\mathrm{aero}} = \boldsymbol{T}_B^L\begin{bmatrix} -A \\ Y \\ N \end{bmatrix}_B = \boldsymbol{T}_B^L q S\begin{bmatrix} -c_A \\ c_Y \\ -c_N \end{bmatrix} \tag{3}$$

The transformation from the body-fixed to the local axis system is carried out using the rotation matrix $\boldsymbol{T}_B^L = (\boldsymbol{T}_L^B)^T$ (Fig. 3),

$$\boldsymbol{T}_L^B = \boldsymbol{T}_1(\Phi)\boldsymbol{T}_2[-(\pi/2) + \Theta]\boldsymbol{T}_1(-\Psi) \tag{4}$$

with

$$\boldsymbol{T}_1(i) = \begin{bmatrix} 1 & 0 & 0 \\ 0 & \cos i & \sin i \\ 0 & -\sin i & \cos i \end{bmatrix}, \qquad \boldsymbol{T}_2(i) = \begin{bmatrix} \cos i & 0 & -\sin i \\ 0 & 1 & 0 \\ \sin i & 0 & \cos i \end{bmatrix} \tag{5}$$

The dynamic pressure is given by

$$q = \tfrac{1}{2}\rho V_a^2 \tag{6}$$

Received 13 July 1998; revision received 24 June 1999; accepted for publication 25 June 1999. Copyright © 1999 by Nicolas Weigel and Klaus H. Well. Published by the American Institute of Aeronautics and Astronautics, Inc., with permission.

*Research Assistant, Institute of Statics and Dynamics of Aerospace Structures.

†Professor and Director, Institute of Flight Mechanics and Control.

Table 1 Mission Data

Parameter	Case 1	Case 2
Orbit 1, altitude of perigee, km	600	800
Altitude of apogee, km	600	800
Inclination, deg	7	98.6
Payload 1, kg	3,000	4,000
Orbit 2, altitude of perigee, km	Free	800
Altitude of apogee, km	35,800	800
Inclination, deg	7	Minimal
Argument of perigee, deg	270	Free
Payload 2, kg	Maximal	4,000

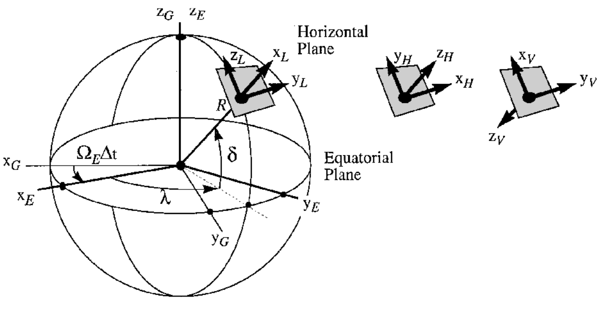

Fig. 1 Local axis system *L*.

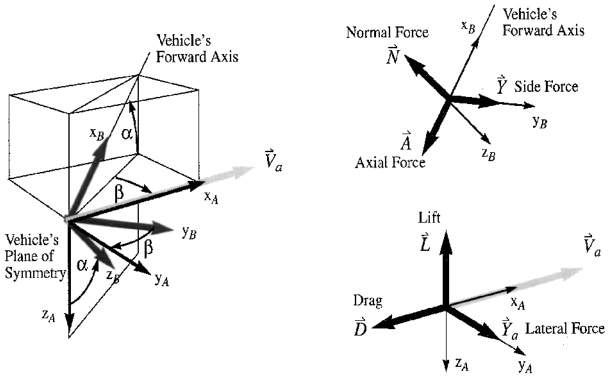

Fig. 2 Air-path system *A* and body-fixed system *B*.

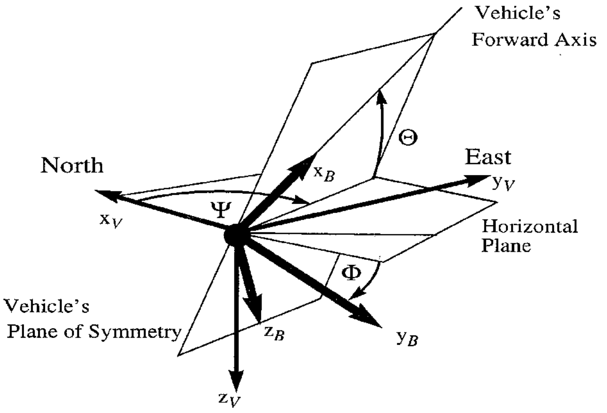

Fig. 3 Body angles Ψ, Φ, and Θ.

where V_a is the air-path velocity

$$\boldsymbol{V}_a = \boldsymbol{V} - \boldsymbol{\Omega}_E \times \boldsymbol{R} - \boldsymbol{V}_W \tag{7}$$

where $\boldsymbol{V}_W$ is the velocity of the atmosphere relative to the planet. The numerical results are computed using the U.S. Standard Atmospheric model of 1976 and a no-wind assumption.

The coefficients c_A, c_Y, and c_N for the example vehicle are taken from Ref. 11 and are shown in Fig. 4. No angle-of-attack dependency of the axial force is considered because the corresponding values were not available for the vehicle. The data are interpolated linearly between data points. This generates some discontinuities in the first derivatives with respect to the control variables that, in general, slows down the convergence speed of the optimization method but does not prevent achievement of a converged solution. Given these aerodynamic coefficients, it has been shown[12] that the vehicle can be trimmed over a wide range of angles of attack and Mach numbers with the available gimballing capability of the rocket engines; this in particular has been checked for the trajectories presented in the present paper.

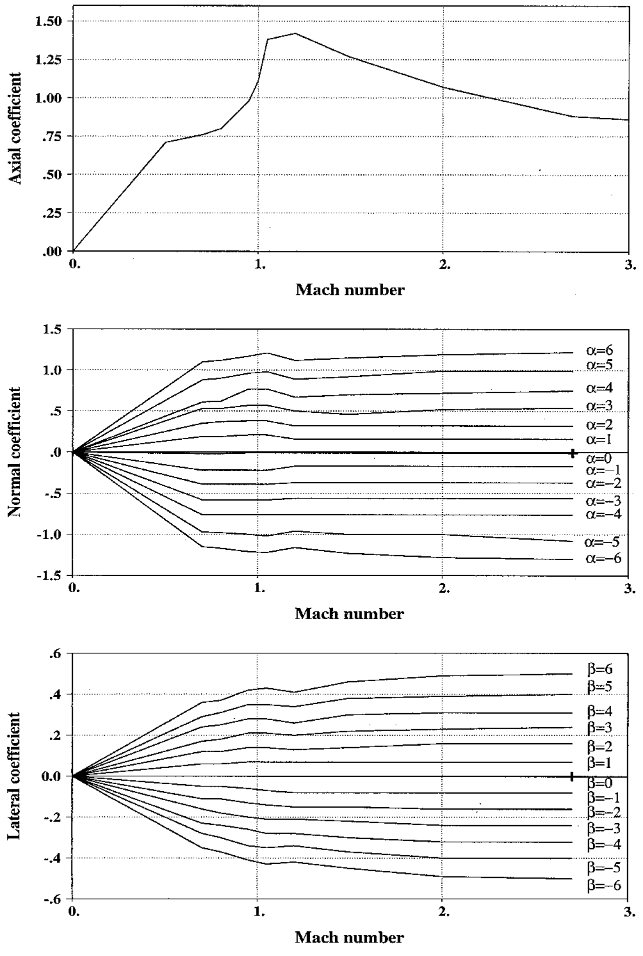

Fig. 4 Aerodynamic coefficients c_A, c_Y, and c_N.

Although the aerodynamics of the empty main stage are important for a precise prediction of the splash-down site, a constant drag coefficient is used in this study due to a lack of data.

Propulsive Forces

The thrust is assumed to point along the vehicle's forward axis. It is, therefore, given in the body-fixed system as

$$\boldsymbol{T} = \begin{bmatrix} A_e(p_e - p) \\ 0 \\ 0 \end{bmatrix}_B - \dot{m}\boldsymbol{V}_e \tag{8}$$

where A_e is the nozzle exit area, p_e the pressure of the exhaust gases, $\dot{m}$ the mass rate, and V_e the velocity of the exhaust gases relative to the vehicle. In the thrust data used, $A_e p_e$ is included in $\dot{m} V_e$ such that

$$\boldsymbol{T} = \begin{bmatrix} -A_e p - \dot{m} V_e \\ 0 \\ 0 \end{bmatrix}_B = \begin{bmatrix} -A_e p - \dot{m} I_{\mathrm{sp}} g_0 \\ 0 \\ 0 \end{bmatrix}_B \tag{9}$$

The propulsive force $\boldsymbol{F}_{\mathrm{prop}}$ in the local axis system L is obtained using the rotation matrix $\boldsymbol{T}_B^L$ defined earlier.

The propulsive system of the Ariane 5 (Ref. 11; see Fig. 5) has three main components.

Table 2 Component masses and constants

Component	Mass
Main stage (H155)	170,000 kg
Dry mass of H155	15,000 kg
Booster (P230)	275,000 kg
Dry mass of P230	39,000 kg
Dry mass of L9.7	3,800 kg
Maximum propellant in L9.7	9,300 kg
μ_E	3.98602×10^{14}, m^3/s^2
R_E	6378.135 km
J_2	1.08263×10^{-3}
Ω_E	7.29246×10^{-5}/s
g_0	9.7983 m/s^2
$\dot{Q}_{\max}$	1135 W/m^2

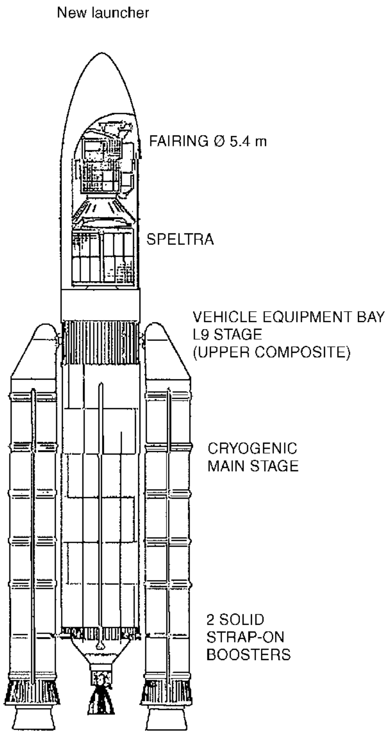

Fig. 5 Ariane 5 launcher.

1) The cryogenic main stage (H155) is powered by a Vulcain engine. It is ignited before liftoff and operates for 570 s.

2) Two solid boosters (P230) are attached to the main stage. Each one operates for 130 s and delivers a varying thrust.

3) The upper composite (L9.7) is equipped with a storage propellant stage delivering a thrust of 28 kN for 1020 s . It can be ignited several times.

The thrust histories are shown in Fig. 6. The thrust time histories of the main stages and the boosters are given for a reference trajectory. It is assumed that this profile will not change significantly for neighboring trajectories. The component's masses are given in Table 2 together with further constants of the problem.

Acceleration of Gravity

The Earth is modeled as an oblate, aspherical planet. Its gravity vector is approximated by expansion into spherical harmonics as follows:

$$g = -\frac{\mu_E}{R^2}\begin{bmatrix} 1 + 1.5J_2(R_E/R)^2(1 - 3\sin^2\delta) \\ 0 \\ J_2(R_E/R)^2 3\sin\delta\cos\delta \end{bmatrix} \tag{10}$$

where $\mu_E = 3.98602e\,14\text{m}^3/\text{s}^2$ is the gravitational parameter, $R_E = 6378.135$ km is the equatorial radius of the Earth, and $J_2 = 1.08263 \times 10^{-3}$ describes its oblateness.

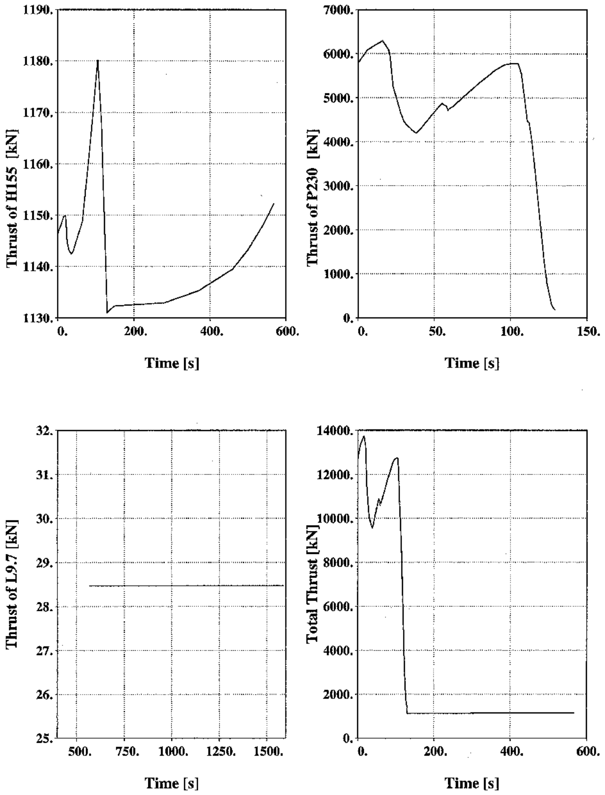

Fig. 6 Thrust histories of H155, P230, and L9.7.

Path Constraints

The ascent trajectories are subject to path constraints. After jettisoning of the payload fairings, the thermal flux has to be bounded,

$$\dot{Q} = 0.5\rho V_a^3 \leq \dot{Q}_{\max} \tag{11}$$

Just after takeoff, the flight-path azimuth angle (degrees) is constrained to values

$$\chi \leq 91.5 \tag{12}$$

This is a precaution taken for the case that an accident takes place less than 60 km after takeoff. It ensures that the impact occurs in the Atlantic Ocean.

Control Inputs

The control inputs for the optimization problem are the yaw angle Ψ, the pitch angle Θ, and the roll angle Φ (Fig. 3). Numerical computations are performed with $\Phi = 0$ because roll is not permitted for the vehicle under consideration. These variables, rather than angle-of-attack and sideslip angle, were chosen because they were more amenable to the vehicle's guidance and control system and could be measured more easily than the aerodynamic angles. Of course, possible angle-of-attack and sideslip-angle constraints must be observed via path constraints. The times for relighting the engines are subject to optimization, too, as variable phase times, as is explained in the following section.

Optimization Problems

Phase Structure

The ascent trajectory of the first problem is subdivided into seven phases, as shown in Table 3. Phases 1–3 describe the ascent of the H155 main stage. They end with booster jettison, payload fairing jettison, and stage separation, respectively. The fourth phase begins with the first ignition of the L9.7 upper composite after stage separation and ends with the injection of the 3000-kg payload into the 600-km circular orbit. Thus, it is subject to boundary conditions corresponding to the orbital elements of the first target orbit. Phase 5 is a ballistic phase needed to satisfy the argument of perigee requirement of the second target orbit. The injection of the second payload into the GTO takes place in phase 6. Its orbital elements are again

Table 3 Summary of case 1

Phase	Duration, s	Characteristics	Boundary constraints	Path constraints
1	0–129	Ends with booster separation	——	$\chi \leq 91.5$ deg
2	129–148	Ends with fairing jettison	$\dot{Q} = 1135\ \mathrm{W\ m^{-2}}$	——
3	148–568	Ends with main stage separation	——	$\dot{Q} \leq 1135\ \mathrm{W\ m^{-2}}$
4	568–628	L9 phase; ends with injection of first payload	$h_{\mathrm{peri}} = 600$ km $h_{\mathrm{apo}} = 600$ km $i = 7$ deg	——
5	628–3225	L9 phase; ballistic phase to ensure argument of perigee	——	——
6[a]	3225–4176	L9 phase; ends with injection of second payload	$h_{\mathrm{apo}} = 35{,}800$ km, $i = 7$ deg, $\omega = 270$ deg	——
7	568–3833	H155 reentry; ends with splash down	Splash down	——

[a] Cost functional $-m_f$.

Table 4 Summary of case 2

Phase	Duration, s	Characteristics	Boundary constraints	Path constraints
1	0–129	Ends with booster separation	——	$\chi \leq 91.5$ deg
2	129–155	Ends with fairing jettison	$\dot{Q} = 1135\ \mathrm{W\ m^{-2}}$	——
3	155–568	Ends with main stage separation	——	$\dot{Q} \leq 1135\ \mathrm{W\ m^{-2}}$
4	568–1268	L9 phase; ends with injection of first payload	$h_{\mathrm{peri}} = 800$ km, $h_{\mathrm{apo}} = 800$ km, $i = 98.6$ deg	——
5	1268–3306	Ballistic phase	——	——
6[a]	3306—3515	L9 phase; ends with injection of second payload	$h_{\mathrm{peri}} = 800$ km, $h_{\mathrm{apo}} = 800$ km	——
7	568–1867	H155 reentry; ends with splash down	Splash down	——

[a] Cost functional i_f.

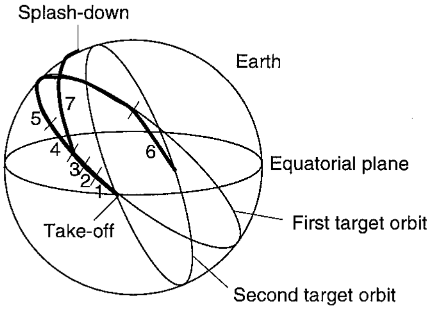

Fig. 7 **Illustration of case 2.**

enforced as boundary conditions. Phase 7 describes the reentry of the burned-out stage. Splash down is required to occur more than 200 km away from a continental coast. Phases 4 and 7 begin simultaneously.

To determine the splash-down location more accurately, the equations of motion of the burned-out stage are integrated numerically rather than using the common Kepler propagation, which neglects the aerodynamic forces.

The phase structure of case 2 as given in Table 4 is similar to that of case 1. Optimal inclination changes are carried out at a latitude of 0° (equator). Because the first orbit is reached at a different latitude, a ballistic flight of the upper stage to the equator takes place in phase 5 (Fig. 7).

The initial mass of the vehicle consists of the total mass of the H155 stage, plus the masses of the two boosters, plus the structural mass of the upper stage, plus the given mass of the first payload, plus the variable mass of the second payload, as well as the variable mass of the fuel for the upper stage. Depending on the particular mission, the optimal initial mass, therefore, is variable.

Cost Functionals

In case 1, the payload injected into the second target orbit (GTO) is to be maximized. This is equivalent to maximizing the total mass at the final time of phase 6 as this is the sum of the payload and the dry mass of the upper composite,

$$C_1 = -m|_{t=t_6} \tag{13}$$

The inclination of the second orbit is to be minimized in case 2,

$$C_2 = i|_{t=t_6}$$

Numerical Solution Procedure

To solve the stated problems, a direct multiple shooting method[6,9] is used. The initial time and the phase separation times are the initial nodes for each phase. Within each phase, additional shooting meshes with gridpoints are defined. At each multiple shooting gridpoint initial states are defined to start the integration over the multiple shooting intervals. These initial conditions are added to the set of optimizable parameters. The numerical integration is performed using a special Runge–Kutta fourth/fifth-order variable stepsize integrator.

Each component of the control vector is approximated within a multiple shooting interval by piecewise linear or piecewise constant functions. To this end, control grids are defined. Each component of the control vector may have its own approximating function and its own control grid. The path constraints are checked at a finite number of points of a separate constraint evaluation grid. Here, the grid is spaced arbitrarily (at the users choice) within each multiple shooting mesh. The same grid is used for all constraints.

The resulting constrained parameter optimization problem is solved using standard sequential quadratic programming solvers such as NPOPT. For details on the numerical optimization method see Ref. 9. The direct multiple shooting method is preferred over, for example, direct collocation as used in OTIS[7] because 1) the transcription method gives greater flexibility in discretizing the continuous optimal control problem, 2) the transcription results in a smaller number of parameters to be optimized by the nonlinear programming solver in comparison to collocation, and 3) the shooting approach gives great flexibility concerning accuracy requirements for integrating the differential equations or constraint satisfaction and/or satisfaction of the optimality criteria.

Numerical Results

Dual Payload Optimization into LEO/GTO (Case 1)

As shown in Table 5, a maximum payload of 2020 kg can be injected into GTO. Splash down of the main stage takes place in the Indian Ocean. The most important control and trajectory data are given in Fig. 8. The control and trajectory histories for case 2 are given in fig. 9. The trajectory is visualized in Fig. 10. The vehicle takes off with 90-deg pitch angle. Pitch then decreases in phases 2–4. The launcher reaches orbital speed in phase 4 as required (see semi-major axis plot). Phase 5 is a coasting phase. In phase 6, the upper composite is injected into GTO with increasing pitch angle.

The main function of the yaw angle consists in modifying the orbit inclination. As shown in Fig. 8, inclination augments steadily from 5.25 deg at takeoff (Kourou's latitude) to 7 deg required by the target orbits, and the yaw angle decreases from initially approximately 90 deg. It is observed that the angle of attack stays below values of approximately 20 deg.

Table 5 Optimization results and splash-down

Parameter	Case 1	Case 2
Orbit 2, payload, kg	Max. 2020	——
Orbit 2, inclination, deg	——	Min. 93.9
Geodetic longitude of splash down, °	54.5	−159.2
Geodetic latitude of splash down, °	2.3	81.6
Location of splash down	Indian Ocean	Arctic sea
Distance of splash-down location from land, km	700	800
Altitude of perigee at stage separation, km	−740	−2253
Altitude of apogee at stage separation, km	646	726

Although the distance of the splash-down location from land is somewhat larger than the permissible value due to the discretization of the coastline, the splash-down constraint is clearly active (Fig. 10).

Because of the relatively low mass of the second payload achieved in case 1, the influence of the target orbit altitude of the first payload is analyzed. To that end, the first payload is injected into a 400-km parking orbit, while the remaining mission data are kept constant (case 1a). Whereas the control and trajectory data are very similar to those of case 1, the upper composite now takes 60 s to inject the first payload rather than 289 s as in case 1. Therefore, a much larger fraction of the propellant can be used to inject the second payload, resulting in an increase of the maximum payload from 2020 to 3473 kg.

Effect of the Splash-Down Constraint on Optimal Trajectories

The splash-down constraint requires 1) the burned-out stage to reenter into the atmosphere and 2) the splash-down site to be located more than 200 km away from a continental coast. The first requirement is fulfilled as long as the perigee at the instant of stage

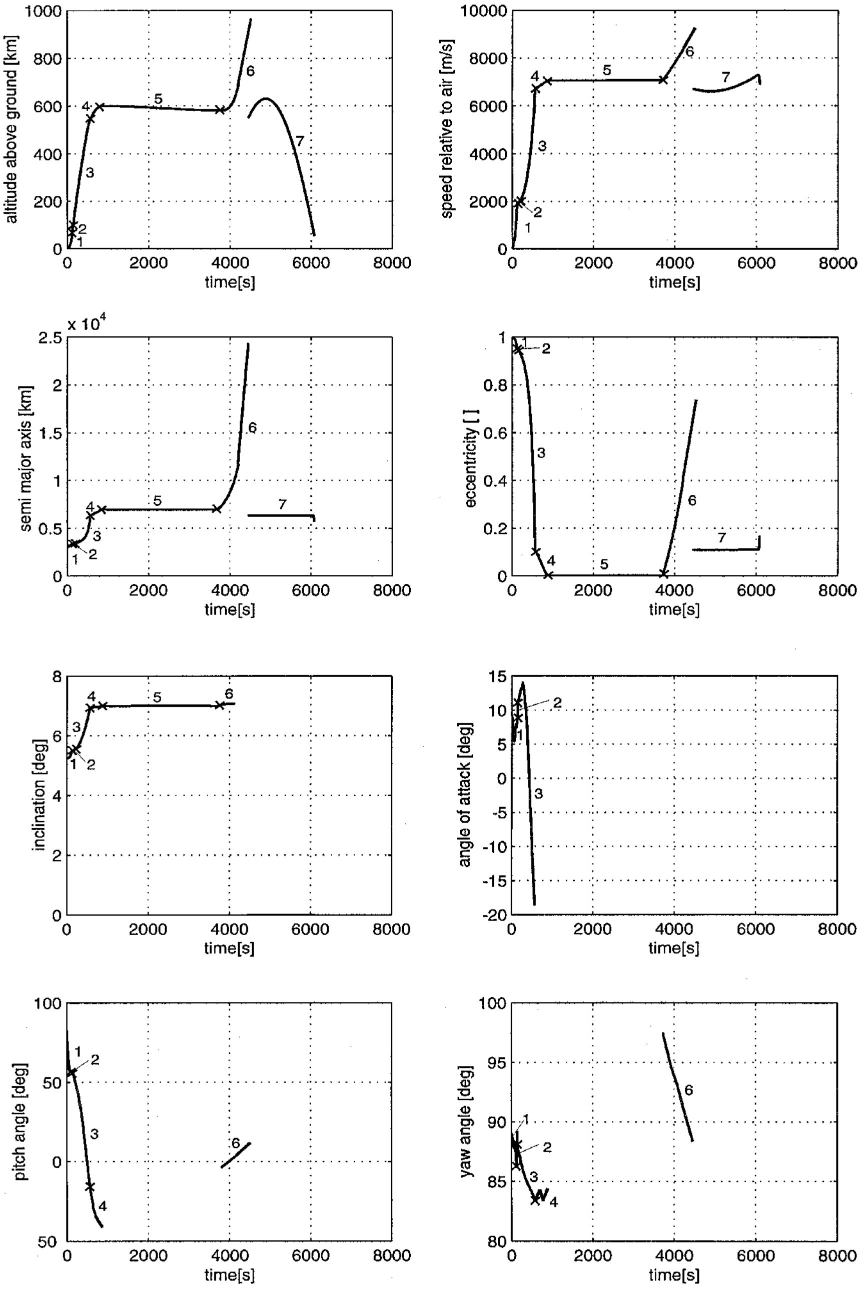

Fig. 8 Case 1: trajectory and control histories.

separation is within the atmosphere. A comparison of the cases 1 (altitude of parking orbit 600 km, altitude of perigee at stage separation −740 km) and 1a (altitude of parking orbit 400 km, altitude of perigee 108 km) suggests that the first part of the constraint has a significant influence on the optimization problem only for low orbits.

To guarantee fulfillment of the splash-down site constraint, it is not sufficient to bound the orbital elements at the instant of stage separation based on a state propagation using Keplerian motion; it is rather necessary to predict the splash-down site by numerically integrating the equations of motion using a realistic aerodynamic model of the empty stage. To analyze the influence of the splash-down site on the optimization result, a simplified five-phase single payload optimization problem derived from case 1 is studied (Table 6). The maximal payload is determined as a function of splash-down location for four permissible splash-down sites (Table 7).

Table 6 Summary of single payload problem

Phase	Characteristics	Boundary constraints	Path constraints
1	Ends with booster separation	——	$\chi \leq 91.5$ deg
2	Ends with fairing jettison	$\dot{Q} = 1135 \text{ W m}^{-2}$	——
3	Ends with main stage separation	——	$\dot{Q} \leq 1135 \text{ W m}^{-2}$
4[a]	L9 phase; ends with injection of payload	$h_{\text{peri}} = 600$ km $h_{\text{apo}} = 600$ km $i = 7$ deg	——
5	H155 reentry; ends with splash down	Splash down	——

[a] Cost functional $-m_f$.

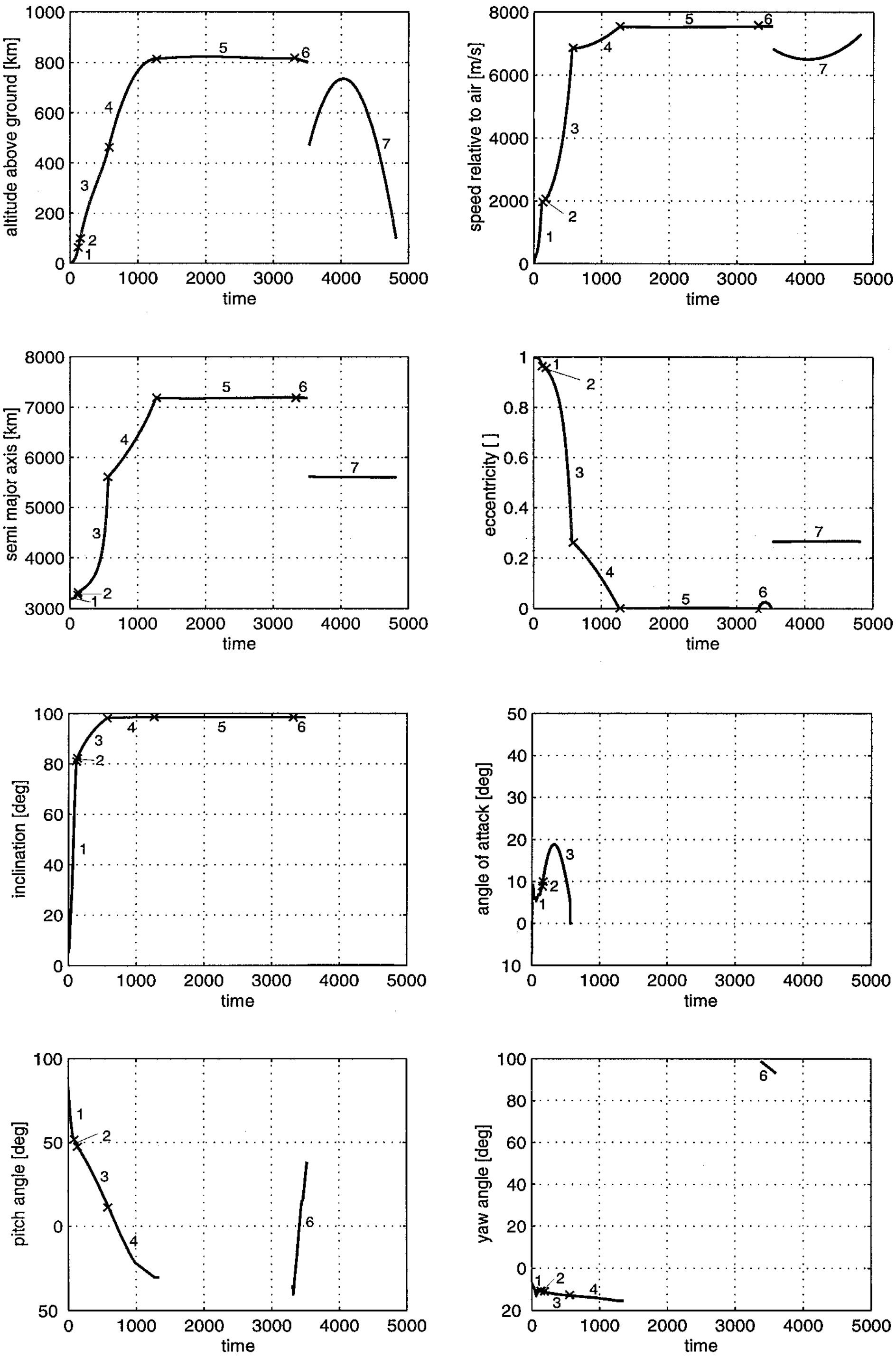

Fig. 9 Case 2: trajectory and control histories.

A more distant splash-down site requires a larger altitude of perigee at stage separation, leading to a larger semimajor axis. As the magnitude of the semimajor axis of an orbit is proportional to its energy level, an extra amount of propellant is needed for distant splash-down sites. Consequently, the payload must be reduced. The data given in Table 7 show the necessity of considering the reentry phase as part of the optimization problem. This permits an accurate determination of the splash-down site, as well as an accurate computation of the payload.

Note that splashdown has to be enforced such that it occurs at least 200 km away from any continental coast, rather than at a predefined location. It is, therefore, not known in advance which continental coast is critical in a given mission. Therefore, we compute a preliminary solution without the splash-down constraint. This yields an unconstrained splash-down location and, therefore, the critical continental coast for example, east Africa in case 1. For the actual solution, the constraint is set according to the preliminary solution.

Maximize the Inclination Difference in Two Circular Orbits (Case 2)

As shown in Table 5, a payload weighing 4000 kg can be injected into a circular orbit with an altitude of 800 km and a minimal inclination of 93.9 deg after injecting another 4000-kg payload into a 800-km SSO. The control and trajectory histories are given in Fig. 9. The trajectory is shown in Fig. 11.

The pitch history is equivalent to that of case 1 for the phases 1–4. However, a pitch angle of 0 deg is expected in phase 6 because both target orbits are circular and have the same altitude. Because of the planet model, the vehicle's distance from the center of Earth increases by 16 km during the ballistic phase. To counterbalance this effect, the pitch angle assumes negative values at the beginning of

Table 7 Splash-down data for four different locations (single payload)

Parameter	Case a	Case b	Case c	Case d
Geodetic longitude of splash down, °	54	85	162	−100
Location of splash down	Western Indian Ocean	Eastern Indian Ocean	Pacific Ocean, near Asia	Pacific Ocean, near Central America
Payload, kg	14,162	13,208	11,324	10,790
Takeoff mass, kg	747,789	745,923	744,596	744,483
Altitude of perigee at stage separation, km	−1,286	−819	−96	96
Altitude of apogee at stage separation, km	650	773	763	645
Semimajor axis at stage separation, km	6,060	6,355	6,712	6,749

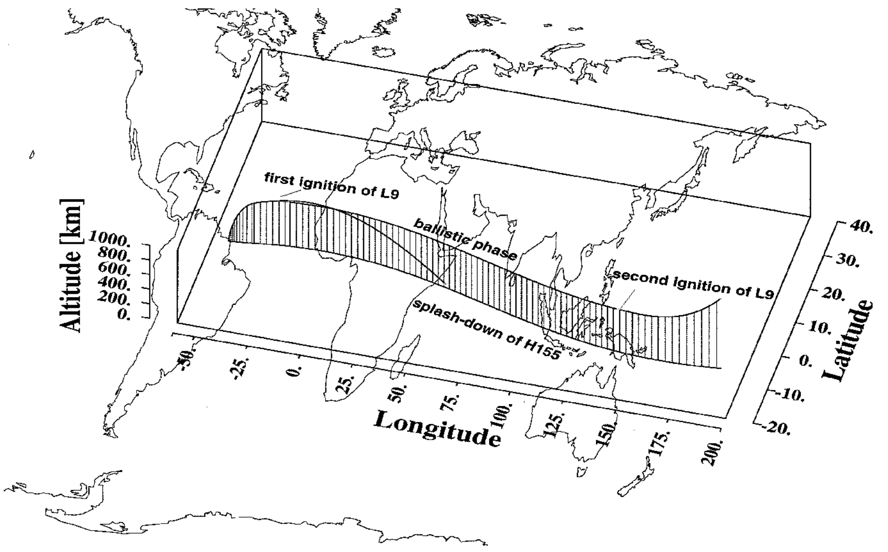

Fig. 10 Case 1: visualization of the trajectory.

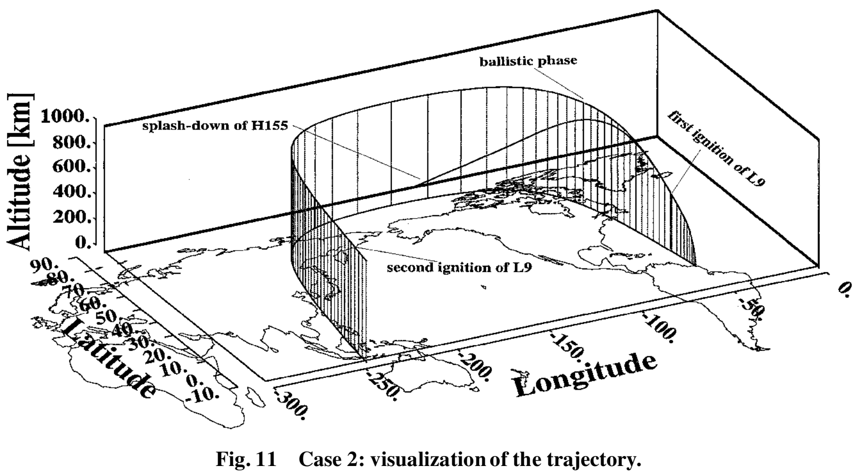

Fig. 11 Case 2: visualization of the trajectory.

phase 6 to decrease the radial velocity component to about −200 m/s. Later, it becomes positive, increasing the radial velocity to 0 m/s (circular target orbit). Inasmuch as the radial velocity is negative during the entire phase, the distance from the center of Earth is corrected.

Generally speaking, inclination changes should be performed at low speed or near one of the orbit nodes. Figure 9 shows that inclination raises sharply in phase 1. It increases much slower in the subsequent phases until reaching 98.6 deg in phase 4 as required.

The comparatively small achievable inclination difference is due to the heavy payloads. It is observed that yaw is approximately 90 deg during the second ignition phase (phase 6). The splash-down constraint does not influence the trajectory noticeably in this case.

Figure 11 shows that the ballistic phase is used to perform an optimal inclination change close to the equator.

Conclusions

Optimal ascent trajectories of a multistage launch vehicle for dual payload injection are considered. The problem is formulated as a multiphase trajectory optimization problem, with one phase representing the reentry trajectory of the burned-out empty main stage of the vehicle. In this way a splash-down position outside of any land mass can be ensured. The maximum payload capability can easily be computed, and it is shown that the computation of a precise splash-down point requires such a reentry simulation. In addition, the sensitivity of the achievable payload with respect to several splash-down positions is determined.

In a second case, the maximum inclination difference of two circular polar orbits for given payload masses is computed. Here, the splash down occurs in the Arctic sea, and the sensitivity of the optimization result with respect to splash-down position is low.

In both examples the computed splash-down positions are based on the assumptions of a constant drag coefficient for the empty stage. This is not quite realistic because the empty stage may tumble and eventually break up into several pieces, thus making the computed splash-down coordinates inaccurate. However, the presented results can serve as a baseline for more detailed simulations taking into consideration all effects that may result in more realistic splash-down positions, for instance, by performing some dispersion analysis.

Although two special problems are treated, the approach presented is rather general and can be used for any multiphase, multibranched trajectory optimization problem with constraints.

References

[1] Well, K. H., and Tandon, S. R., "Rocket Ascent Trajectory Optimization via Recursive Quadratic Programming," *Journal of Astronautical Sciences,* Vol. 30, No. 2, 1982, pp. 101–116.

[2] Landiech, P., and Aumasson, C., "Optimal Trajectory of Ariane 5 Type Launcher with First Stage Fallout Constraints," International Astronautical Federation, Paper 86-230, Oct. 1986.

[3] Flury, W., and Hechler, M., "Efficient Calculation of Ariane Ascent Trajectories with Recursive Quadratic Programming," European Aerospace Conf., Paper EAC-89-63, May 1989.

[4] Well, K. H., "Ariane 5 Ascent Trajectory Optimization with a First-Stage Splash-Down Constraint," *Proceedings of 8th International Federation of Automatic Control Workshop on Control Application*, Paris, 1989; also TR IFR-99-04, Inst. for Flight Mechanics and Control, Univ. of Stuttgart, Oct. 1999.

[5] Spangelo, I., and Well, K. H., "Rocket Ascent with Heat-Flux and Splash-Down Constraints," Reprints of the 13th IFAC Symposium on Automatic Control in Aerospace, edited by D. B. Schaechter, K. R. Lovell, Lockheed Missile and Space Company, Inc., Sunnyvale CA, Sept. 1994, pp. 8–14.

[6] Bock, H. G., and Plitt, K. J., "A Multiple Shooting Algorithm for Direct Solution of Optimal Control Problems," *Preprints of International Federation of Automatic Control*, Pergamon Press, New York, 1984, pp. 243–247.

[7] Hargraves, C. R., and Paris, S. W., "Direct Trajectory Optimization Using Nonlinear Programming and Collocation," *Journal of Guidance, Control, and Dynamics*, Vol. 10, No. 4, 1987, pp. 338–342.

[8] Buhl, W., Ebert, K., Herbst, H., Röllecke, E., Berger, E., Crues, E., Jänsch, C., Schnepper, K., and Well, K. H., "ALTOS—Ein Softwarepaket zur Aufstiegsbahnoptimierung von konventionellen und zukünftigen Trägersystemen," Deutsche Gesellschaft für Luft-und Raumfahrt–Jahrbuch 1991, Berlin, Sept. 1991 (in German).

[9] Jänsch, C., Schnepper. K., Well, K. H., and Gonzales, A. L., "Multiphase Trajectory Optimization Methods with Applications to Hypersonic Vehicles," *Applied Mathematics in Aerospace Science and Engineering*, edited by A. Miele and A. Salvetti, Plenum, New York, 1994, Chap. 8.

[10] Betts, J. T., and Huffman, W. P., "Path Constrained Trajectory Optimization Using Sparse Sequential Quadratic Programming," *Journal of Guidance, Control, and Dynamics*, Vol. 16, No. 1, 1993, pp. 59–68.

[11] "Characteristiques Propulsives et Aerodynamiques du Lanceur Ariane 5 et Elements Generales des Trajectoires," ESA TN D/STS-AD, 1987 (in French).

[12] Eckstein, J., "Aerodynamik-Modell und Entwurf einer Nicklageregelung für eine Ariane 5 Trägerrakete," Internal Rept., Inst. of Flight Mechanics and Control (IFR), IFR-95-002, Univ. of Stuttgart, Stuttgart, Germany, 1995 (in German).